

Oxidation and Kinetic Analysis of Pure Aluminum Powder under Non-isothermal Condition

Hasani S*, Panjepour M and Shamanian M

Department of Materials Engineering, Isfahan University of Technology, 84156-83111, Isfahan, Iran

Abstract

The non-isothermal oxidation of aluminum particle powders (100-200 μm) was investigated by simultaneous Thermogravimetry (TG) and Differential Thermal Analysis (DTA) under linear temperature programming (from 25°C up to 1400°C) at different heating rates (10, 20 and 30°C/min). Phase and structural evolution were studied by X-Ray Diffraction technique (XRD) and Scanning Electron Microscopy (SEM). It was found that the oxidation of aluminum powders took place during several stages and the complete oxidation process did not happen even up to 1400°C. Among different stages, the temperature ranging from 1000 to 1150°C was identified as the main stage for oxidation process. Hence, only kinetic analysis of non-isothermal in this region was determined by a new simple method. Consequently, the results of the kinetic analysis in a form of kinetic triplet were obtained:

$f(\alpha) = -1/\ln(1-\alpha)$, $E \approx 435$ (kJ/mol) and $A \approx 0.9 \times 1020$ (min^{-1}). In addition, the method was validated by the mechanism obtained through experimental study.

Keywords: Aluminum powder; Oxidation; Kinetic analysis; Non-isothermal; XRD; SEM; TG-DTA

Introduction

Mechanism of Aluminum particles oxidation plays an important role in development of aluminothermic processes. Of the special features of the oxidation process of aluminum powders is the oxidation enthalpy and high combustion temperature, its rather low costs, and the production of safe products for the ecosystem [1]. For this reason, aluminum powders have been widely used for aluminothermic reactions, fuel additive in propellants, explosives, and pyrotechnics within the recent few decades [2-4]. Due to the wide range application of the aluminum powders oxidation, many studies have been done in this area. As an example, through the studies performed in 2000 and 2002, it was found that at low temperatures ($T < 573\text{K}$), a thin layer of amorphous aluminum oxide is formed on the surface of the aluminum particles. With a low thickness, this amorphous oxide film contained more aluminum than the Al_2O_3 composition (non-stoichiometric Al_2O_3) which was thermodynamically more stable than its crystalline state unless it reached a critical thickness [5-7]. On the other hand, the presence of more aluminum in the structure of the layer, prevents from crystallization of amorphous alumina crust. When the thickness of the amorphous alumina layer reached a critical value (from 0.5 nm [8] to 4 nm [9] in higher temperature ($T < 573\text{K}$), it was changed into an alumina with a $\gamma\text{-Al}_2\text{O}_3$ crystalline structure [7]. By the formation of the crystalline structure of $\gamma\text{-Al}_2\text{O}_3$ phase, a network of grain boundaries are formed within the oxide crust, which leads to the increase of oxidation rate [10] due to the increase in the oxygen diffusion paths [11]. By continuing the oxidation process at this stage, the quick penetration paths on the $\gamma\text{-Al}_2\text{O}_3$ layer are closed and hence the oxidation rate is reduced again [10]. Under this condition, the $\gamma\text{-Al}_2\text{O}_3$ phase is changed to $\alpha\text{-Al}_2\text{O}_3$ phase by increasing the temperature. The $\alpha\text{-Al}_2\text{O}_3$ phase can be created either directly from the transformation of $\gamma\text{-Al}_2\text{O}_3$ phase or indirectly from the transformation of θ and δ intermediate phases. Since the density of the γ , θ and δ phases are approximately the same, thereby no significant change occurs in the oxidation process in the phase transformation [12]. Finally, by the start of ignition temperature and with regard to the particles size, intense oxidation takes place within the particles in continuation [10].

Despite the studies and investigations performed in this area, the effect of aluminum smelting on the aluminum powders oxidation process have not been studied in details. It also seems that there are some obscurities about the conformity of laboratory results with the proposed oxidation mechanism and its kinetic study. It is therefore required to do a comprehensive study in this area.

The aim of this study is to employ thermal analysis studies (TG-DTA), Scanning Electron Microscope (SEM) and X-Ray Diffraction (XRD), to determine the kinetics of aluminum powder particles oxidation.

Materials and Experimental Methods

The aluminum powder (produced by Fluka Company) with a purity of more than 99% and grain size of 100-200 μm was used in this study. To study the mechanism of aluminum oxidation, the experiments were carried out in a Simultaneous thermal analysis (STA) device (STA503, Bahr), capable of simultaneous DTA-TG analysis at a temperature ranging from 25 to 1500°C. The aluminum powder samples were oxidized directly (under air atmosphere) within the STA device, at a temperature ranging from ambient temperature to 1400°C, using various heating rates: 10, 20 and 30°C/min. The sample mass used for the experiments was about 35.5 ± 0.5 mg. In the next stage, the products obtained from this process were studied for their microstructure and phase analysis by SEM (XL30 SERIES, Philips) and XRD (MPD-XPRT, Philips).

*Corresponding author: Saeed Hasani, Department of Materials Engineering, Isfahan University of Technology, Tel: +98-3113915739; Fax: +98-3113912752, E-mail: s.hasani@ma.iut.ac.ir

Received March 08, 2011; Published October 22, 2012

Citation: Hasani S, Panjepour M, Shamanian M (2012) Oxidation and Kinetic Analysis of Pure Aluminum Powder under Non-isothermal Condition. 1:385. doi:10.4172/scientificreports.385

Copyright: © 2012 Hasani S, et al. This is an open-access article distributed under the terms of the Creative Commons Attribution License, which permits unrestricted use, distribution, and reproduction in any medium, provided the original author and source are credited.

Results and Discussion

Thermal analysis

The curves of DTA and TG are depicted in Figures 1 and 2 respectively. Figure 3 is also presented to better understand and gain enough recognition of the phenomena performed based on these curves, with the characteristic temperatures of oxidation process (T_1 to T_7). According to this figure, each DTA-TG curve can be divided into different regions.

These regions are respectively as follows:

Region I: No noticeable mass gain (Δm) and heat flow (DTA (μV)) changes are observed by increasing the temperature from 25°C to T_1 .

$$\Delta m = m_t - m_0 \quad (1)$$

Where m_t is the mass of the sample at arbitrary time t (or temperature T), and m_0 is the mass of the sample at the beginning of the reaction.

Region II: By the passage of T_1 , Δm increases and heat flow (in the form of exothermic peak up to 660°C) is noticeable. By increasing the heat up to T_4 , there is a continuous Δm increase in the TG curve. While, in its corresponding DTA curve, the above exothermic peak is suddenly affected by the latent heat of melting aluminum at 660°C. In other words, this phenomenon is indicative of the overlapping of two exothermic (resulting from oxidation process) and endothermic peaks (resulting from the aluminum melt). As it is observed in this region, the intensity of the endothermic process of the aluminum melt has overshadowed the exothermic process of oxidation. Finally, this region is terminated at T_4 .

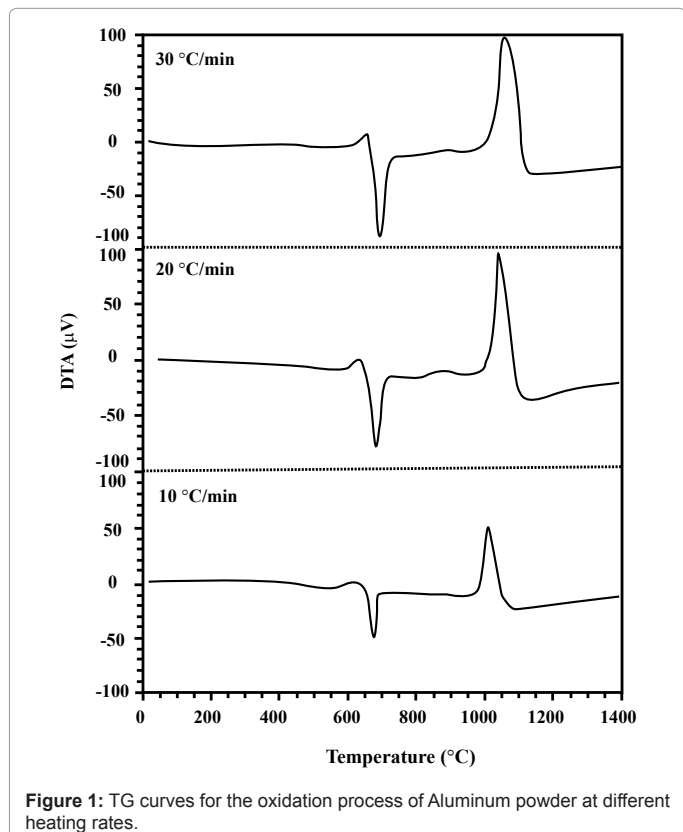


Figure 1: TG curves for the oxidation process of Aluminum powder at different heating rates.

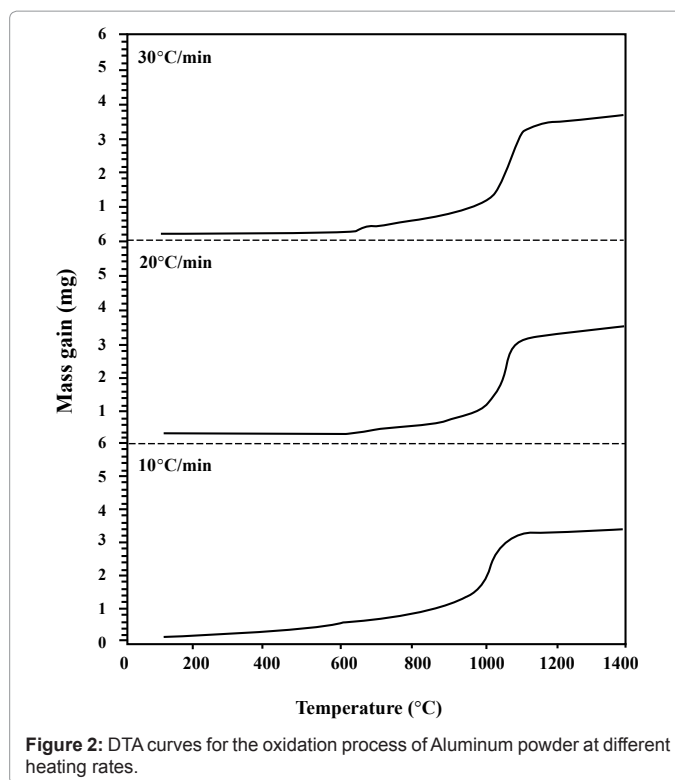


Figure 2: DTA curves for the oxidation process of Aluminum powder at different heating rates.

Region III: By an increase in temperature from T_4 to T_6 no noticeable Δm and heat flow is observed.

Region IV: By the passage of temperature from T_6 , a noticeable increase in Δm as well as in heat flow (in the form of exothermic peak) is obtained.

Region V: From T_7 to 1400°C, no noticeable change is observed in any of the curves.

As it is observed in figures 1 and 2, while DTA-TG curves are at different heating rates, no change takes place in the course of the stages of the oxidation process of aluminum powders. Table 1 shows the influence of heating rate on the characteristic temperatures and Δm at two regions of II and IV ($\Delta m_{II} = \Delta m|_{T_4} - \Delta m|_{T_1}$ and $\Delta m_{IV} = \Delta m|_{T_7} - \Delta m|_{T_6}$). Increasing the heating rate leads to the increase in T_1 to T_7 , Δm_{II} and Δm_{IV} values.

Microstructure observations

Microscopic images of the particles which experienced regions I, II and IV, are presented in figures 4, 5 and 6 respectively. The morphology of the particles of aluminum powders in ambient temperature is shown in figure 4. As it is observed in this figure, the surfaces of these particles are so smooth which confirms the amorphous structure of the oxide crust of aluminum particles. In figure 5, the morphology of an aluminum particle after being exposed to region II and cooled up from 900°C to the ambient temperature is depicted. As shown, since the structure of oxide crust is crystalline, its grain structure and grain boundary are therefore clearly observable. figures 6(a) and (b) show the morphology of aluminum powder particles after passing through region IV. In figure 6(a), the permeation of melted aluminum to the outside of oxide crust (especially on the location of grain boundary)

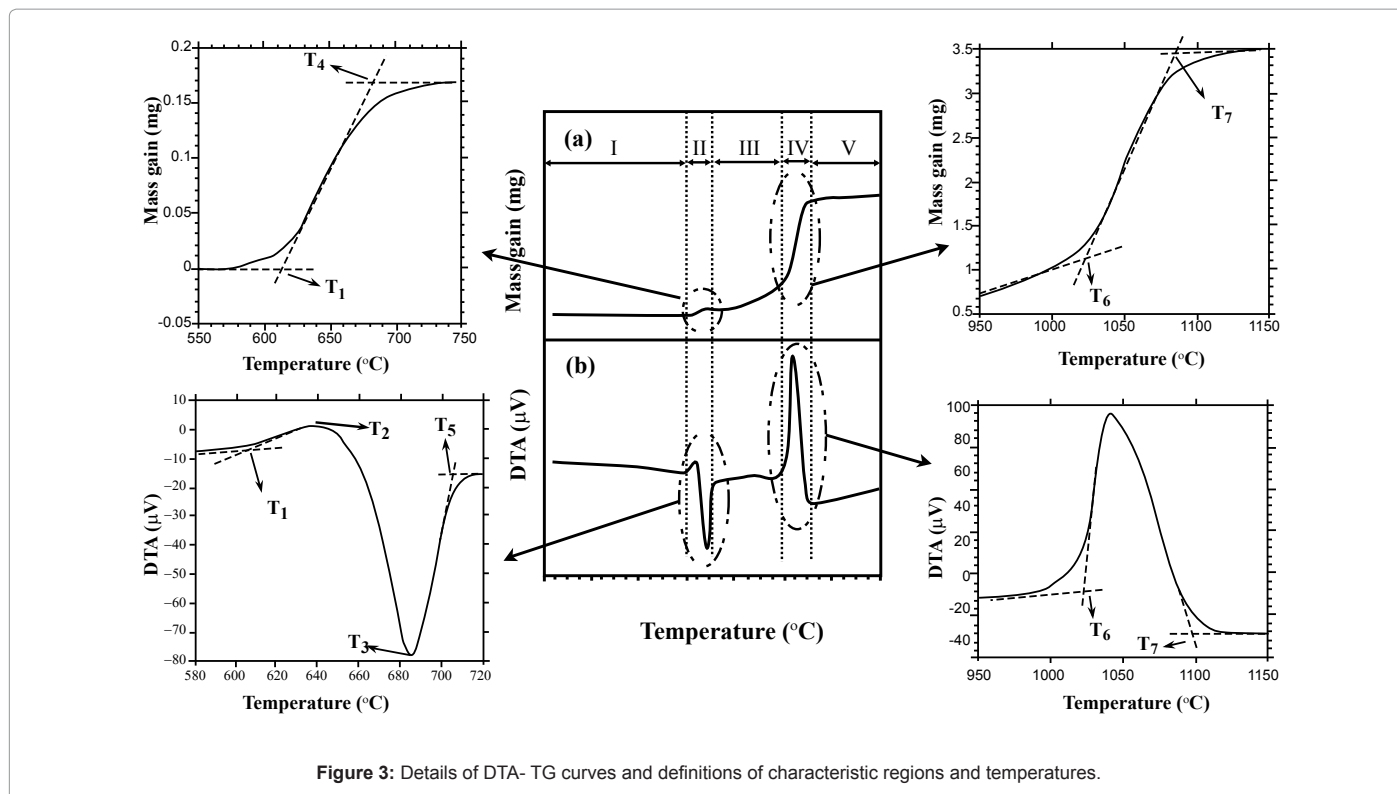


Figure 3: Details of DTA- TG curves and definitions of characteristic regions and temperatures.

Heating rate (°C/min)	(°C) T_1	(°C) T_2	(°C) T_3	(°C) T_4	(°C) T_5	(°C) T_6	(°C) T_7	Δm_{II} (mg)	Δm_{IV} (mg)
10	590	616	676	680	683	990	1070	0.10	1.3
20	610	640	685	687	705	1025	1090	0.15	2.2
30	616	653	695	700	713	1030	1120	0.20	2.3

Table 1: The influence of heating rate on the characteristic temperatures and Δm differences at the two regions of II and IV.

and then its immediate oxidation are clearly shown. Figure 6(b) also shows the burst of an aluminum particle and the remaining part of the torn oxide crust.

Phenomena occurring in the course of heating

The results obtained from the DTA-TG curves (presented in figures 1 and 2) for region I clearly show that under T_1 , there is no phenomenon resulting in these curves. Considering these results, it can be said that due to the absence of any crystalline structure (Figure 4), the amorphous oxide crust protect the remaining aluminum against more oxidation. Therefore, within this temperature range, no noticeable increase in Δm has been taken place, which is indicative of any oxidation. The studies performed by Jeurgens et al. [8] also support this claim. In addition, according to figure 7(a), the XRD pattern of the aluminum particles at ambient temperature contains only Aluminum peaks and no peak is observed indicating the presence of any oxide phases.

As can be seen, in region II, Δm increases which indicates aluminum oxidation process (Table 3). Additionally, with regard to the occurred process in this region, at $T > 660^\circ\text{C}$, the aluminum in the oxide crust is as a melt phase, which its volume expansion coefficient is greater than the solid state. In other word, this melt can affect the outer oxide crust by tensions resulting from its expansion.

By referring to figure 5, it is observed that the morphology of oxide crust is completely transformed from amorphous state to a

crystalline structure. Therefore, oxidation at region II can be indicative of the crystallization of the amorphous oxide layer, due to the grain boundaries formation at the oxide layer structure, which can prepare rapid diffusion paths for the oxidation of aluminum. The studies performed by Levin et al. [12], specified that the amorphous oxide layer is transformed to crystalline $\gamma\text{-Al}_2\text{O}_3$ which has a higher density (about 20%) than the amorphous state. So, during this transformation, micro-cracks formation in the oxide crust is inevitable. Hence, the presence of these micro-cracks and grain boundaries has facilitated the oxidation in region II. But, in region III, the above diffusion paths will be destroyed as a result of oxidation process so that the rate of oxidation is abruptly reduced. Therefore, there is no noticeable sign of increase in Δm .

The issue ignored by researchers is the situation of the liquid aluminum at 660°C , which remains imprisoned inside the oxide crust. By increasing the temperature, the liquid aluminum starts to expand and as a result, an added tension is applied on the crust. The tension resulting from this expansion up to 1000°C (region IV) succeeds in tearing the oxide layer. Then, by the permeation of melted aluminum to outer part of the crust and then in contact with the atmosphere, a severe oxidation takes place. This oxidation is accompanied with great heat flow resulting in considerable increase of Δm (Table 3). By the continuation of oxidation in this region, the cracks resulting from the tearing of oxide layer is repaired and inner aluminum is protected against oxidation. The result of XRD pattern (Figure 7(b)) of the products experienced this region, proves the presence of the remaining

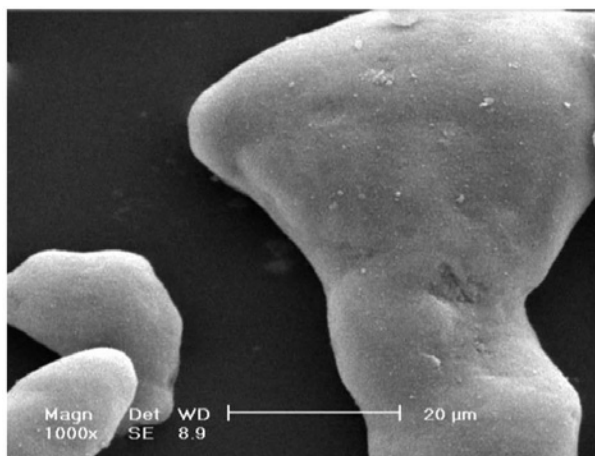


Figure 4: A SEM micrograph of the particles of aluminum powders before experiment.

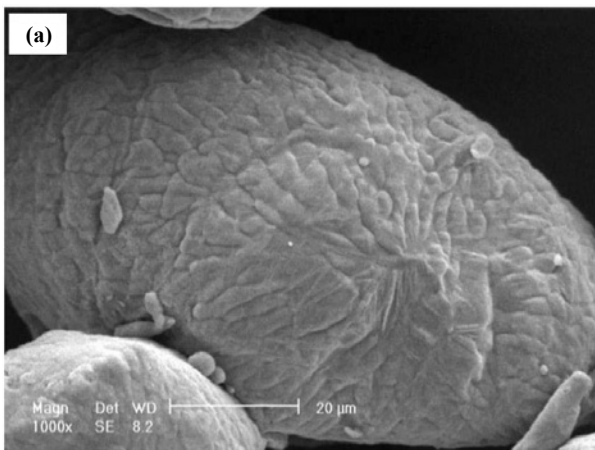


Figure 5: SEM micrographs of an aluminum particle after being exposed to region II and cooled up from 900°C to the ambient temperature, at the various magnifications.

aluminum in the products. This phenomenon is well proved by referring to the oxidation rate at region V and the morphology presented in figure 6(a). In addition, it is demonstrated that the mechanism of oxidation on the surface of aluminum particles is diffusion controlled.

Therefore, the value of Δm produced in the samples show that the complete oxidation of aluminum powder particles does not take place even up to 1400°C. If the particles were completely oxidized (i.e. Δm is equal up to 31 mg), the final Δm must have been reported to be greatly more than the value depicted in the TG curves.

Kinetic analysis

As it is presented in DTA and TG curves in figures 1 and 2, the main part of the oxidation process is carried out within the range of 1000-1150°C (region IV). Therefore, only the kinetic study of this region (non-isothermal kinetic analysis) is performed.

The fractional reaction (α) can easily be specified at this stage by TG curves (Figure 2) and following equation [13-15]:

$$\alpha = \frac{\Delta m|_T - \Delta m|_{T_6}}{\Delta m_{IV}}, T_6 < T < T_7 \quad (2)$$

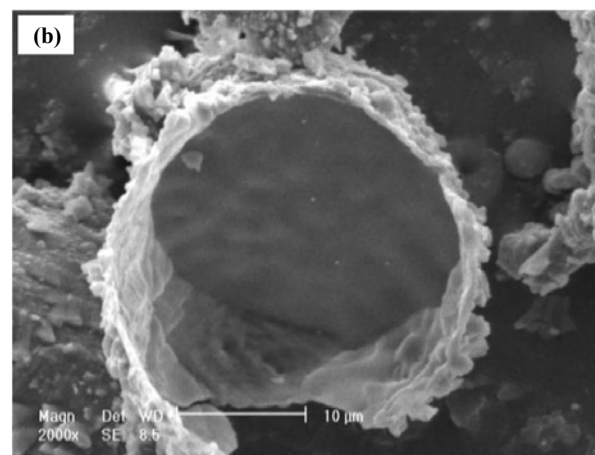
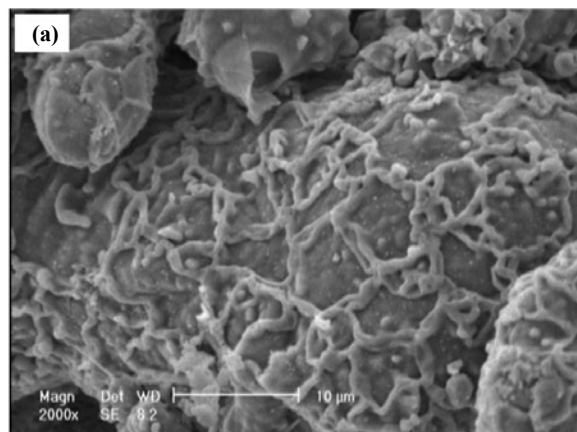


Figure 6: SEM micrographs of aluminum powder particles after passing through the region IV

a) the permeation of melted aluminum to the outside of the oxide crust (especially on the location of grain boundary) and its oxidation immediately after exiting the crust and b) the burst of an aluminum particle and the remaining part of the torn oxide crust.

Where $\Delta m|_T$ represents the mass gain of sample at arbitrary time t (or temperature T).

The curves of α versus T at different heating rates for the oxidation reaction of aluminum powder (through region IV) are shown in figure 8. It is also of great importance that there is a possibility of obtaining the curves of α by the area under the DTA curves [16,17]. The curves of α extracted from the TG and DTA curves are presented in figure 9. As it is observed, there is a good conformity among the results obtained from the two methods.

The curve α versus T can be used for the kinetic analysis and the description of the reaction mechanism. For this purpose, it is possible to analyze the non-isothermal kinetic data by combining the equations below:

1) The differential form of the kinetic equation:

$$d\alpha / dt = k \cdot f(\alpha) \quad (3)$$

Where,

t : time,

k : reaction rate constant,

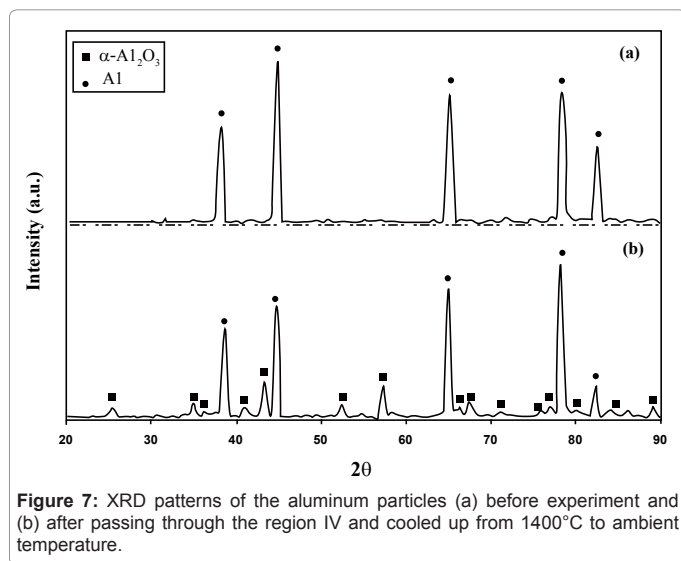


Figure 7: XRD patterns of the aluminum particles (a) before experiment and (b) after passing through the region IV and cooled up from 1400°C to ambient temperature.

No.	Symbol	Reaction Model	Differential Reaction Model $f(\alpha)$
1	P1	Power law	$4\alpha^{3/4}$
2	P2	Power law	$3\alpha^{2/3}$
3	P3	Power law	$2\alpha^{1/2}$
4	P4	Power law	$2 / 3\alpha^{-1/2}$
5	R1	Zero-order (Polanyi-Winger equation)	1
6	R2	Phase-boundary controlled reaction (contracting area, i.e. bidimensional shape)	$2(1-\alpha)^{1/2}$
7	R3	Phase-boundary controlled reaction (contracting volume, i.e. tridimensional shape)	$3(1-\alpha)^{2/3}$
8	F1	First-order (Mampel)	$(1-\alpha)$
9	F3/2	Three-halves order	$(1-\alpha)^{3/2}$
10	F2	Second-order	$(1-\alpha)^2$
11	F3	Third-order	$(1-\alpha)^3$
12	A1/2	Avarmi-Erofe'ev ($r = 0.5$)	$(1/2)(1-\alpha)[-\ln(1-\alpha)]^{-1}$
13	A3/2	Avarmi-Erofe'ev ($r = 1.5$)	$(3/2)(1-\alpha)[-\ln(1-\alpha)]^{1/3}$
14	A2	Avarmi-Erofe'ev ($r = 2$)	$2(1-\alpha)[-\ln(1-\alpha)]^{1/2}$
15	A3	Avarmi-Erofe'ev ($r = 3$)	$3(1-\alpha)[-\ln(1-\alpha)]^{2/3}$
16	A4	Avarmi-Erofe'ev ($r = 4$)	$4(1-\alpha)[-\ln(1-\alpha)]^{3/4}$
17	D1	One-dimensional diffusion	$1 / 2\alpha$
18	D2	Two-dimensional diffusion (bidimensional particle shape) Valensi equation	$1 / [-\ln(1-\alpha)]$
19	D3	Three-dimensional diffusion (tridimensional particle shape) Jander equation	$3(1-\alpha)^{1/3} / [2((1-\alpha)^{-1/3} - 1)]$
20	D4	Three-dimensional diffusion (tridimensional particle shape) Ginstling-Brounshtein	$3 / 2[(1-\alpha)^{-1/3} - 1]$

Table 2: Algebraic expressions of $f(\alpha)$ for the kinetic models considered in this work in the solid state reactions [14].

$f(\alpha)$: an algebraic function depending on the reaction mechanism (or differential reaction model).

2) The Arrhenius equation:

$$k = A \cdot \exp(-E / RT) \quad (4)$$

Where A (the pre-exponential factor) and E (the activation energy) are the Arrhenius parameters, T and R are absolute temperature and gas constant, respectively.

3) The equation of the temperature changes in terms of time:

$$T = T_0 + \beta \cdot t \quad (5)$$

Where T_0 is the initial temperature and β is constant heating rate.

Therefore, with a view to equation (5) we will have:

$$dT / dt = \beta$$

$$\text{i.e. } dt = dT / \beta \quad (6)$$

The basic kinetic equation for non-isothermal kinetic data is thus obtained by combining equations (3), (4) and (6).

$$d\alpha / dT = (A / \beta) \cdot \exp(-E / RT) \cdot f(\alpha) \quad (7)$$

Equation (7) cannot be integrated analytically and hence some of the methods of approximate solution of the equation (i.e. the model-free and model-fitting methods) were proposed by several workers. All these methods aim to determine a sufficient number of kinetic parameters, usually at least the Arrhenius parameters and a conversion function or kinetic model, so that accurate extrapolations of kinetic behavior can be made [18-22]. But, in many model-free methods (e.g. isoconversional methods), too much attention is focused on the estimation of only Arrhenius parameters without choosing the kinetic model. In fact, these methods postpone the problem of identifying a suitable kinetic model until an estimate of the activation energy has been made. A major reason for doing this, is that misidentification of the kinetic model has a great effect on the values obtained for the Arrhenius parameters in both isothermal and non-isothermal kinetic analyses [23]. For this reason, in this research, a new simple method (as a linear approximation method [24] for approximate solution of equation (7) is presented. This method uses for non-isothermal data (alpha against temperature) is obtained at different heating rates, in order to determine the kinetic triplets ($f(\alpha)$, E , and A) at any particular value of α . As it is observed in figure 8, all of the central sections of the curves ($0.1 < \alpha < 0.9$) are linear. So, based on this method, these sections can be obtained by deleting the initial and final sections of the reaction, and $d\alpha/dT$ term in equation (7) can be determined by using this equation:

$$d\alpha / dT = C \quad (8)$$

Where C is the slope of a straight line (the central section of α vs. T curve).

Consequently, equation (7) can be rewritten as follows:

$$f(\alpha) = (\beta \cdot C / A) \cdot \exp(E / RT) \quad (9)$$

Or;

$$\ln f(\alpha) = \ln(\beta \cdot C / A) + (E / RT) \quad (10)$$

Hence, plotting the left hand side of equation (10), which includes $\ln f(\alpha)$ against $1/T$, gives a straight line with a slope of E/R from which E is obtained. Whereas, intercept is equal to $\ln(\beta \cdot C / A)$ by which A can be calculated.

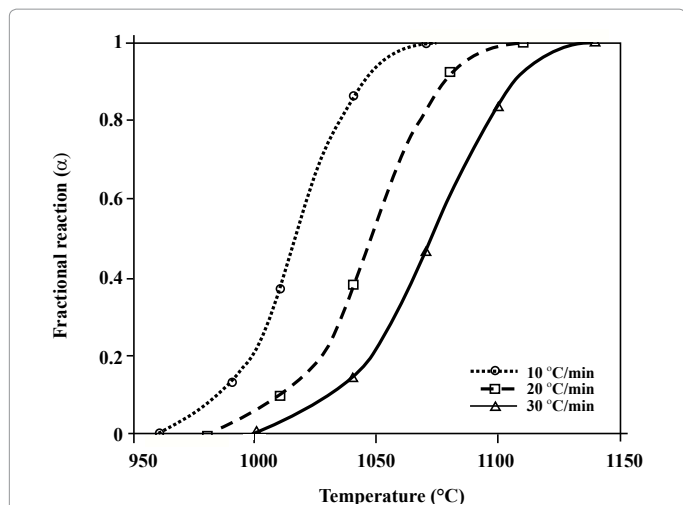


Figure 8: The α versus T curves for the oxidation reaction of aluminum powder through region IV, obtained at different heating rates (extracted from TG curves).

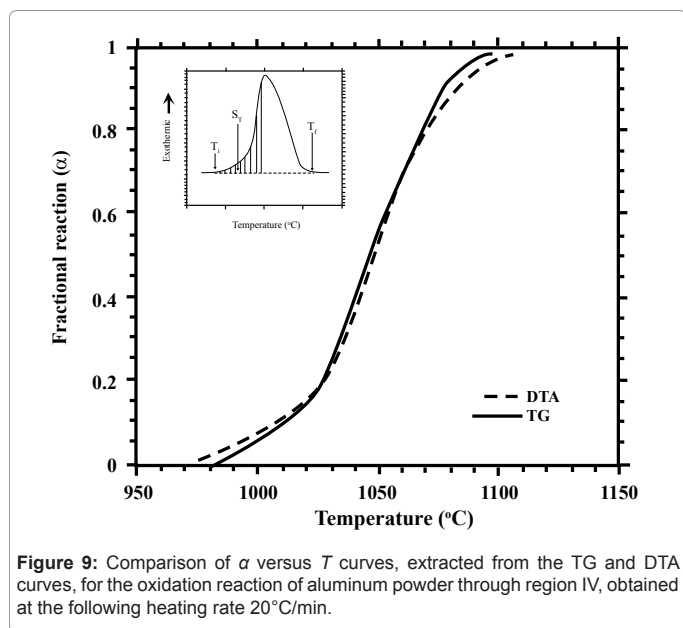


Figure 9: Comparison of α versus T curves, extracted from the TG and DTA curves, for the oxidation reaction of aluminum powder through region IV, obtained at the following heating rate 20°C/min.

Since there is no a priori knowledge about the kinetic model of oxidation of aluminum powders, several widely used gas-solid kinetic models or reaction models, $f(\alpha)$, have been considered. These are diffusion-controlled model, phase boundary model, order of reaction model, and nucleation and growth model as summarized in table 2 [17]. Thereafter, the oxidation mechanism of aluminum is obtained by replacing different $f(\alpha)$ functions in equation (10). For this purpose, versus $1/T$ curves were drawn with regard to different $f(\alpha)$ (according to Table 2). In fact, in exchange for $f(\alpha)$, the model that gives the best linear fit is selected as a chosen kinetic model. According to figures 10 and 11, a correlation coefficient analysis indicates that the best linear fit is obtained with two-dimensional diffusion controlled equation (in table 2 presented by D2) having the highest correlation coefficient values (greater than 99%). The related equation for this mechanism is:

$$f(\alpha) = -1 / \ln(1 - \alpha) \quad (11)$$

Figure 11 depicts the $\ln[-1 / \ln(1 - \alpha)]$ curves in terms of $1/T$

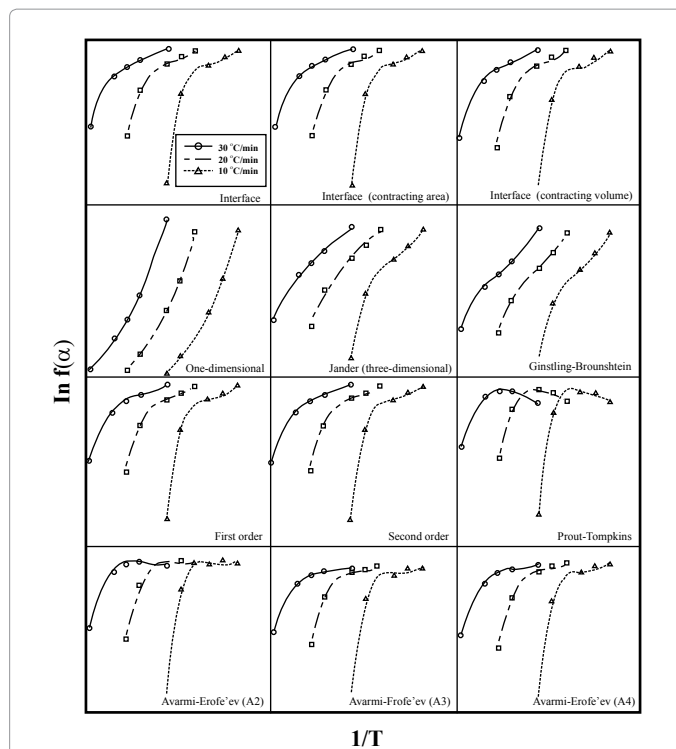


Figure 10: The curves of $\ln f(\alpha)$ versus $1/T$ for different kinetic models using values of α extracted from Figure 8.

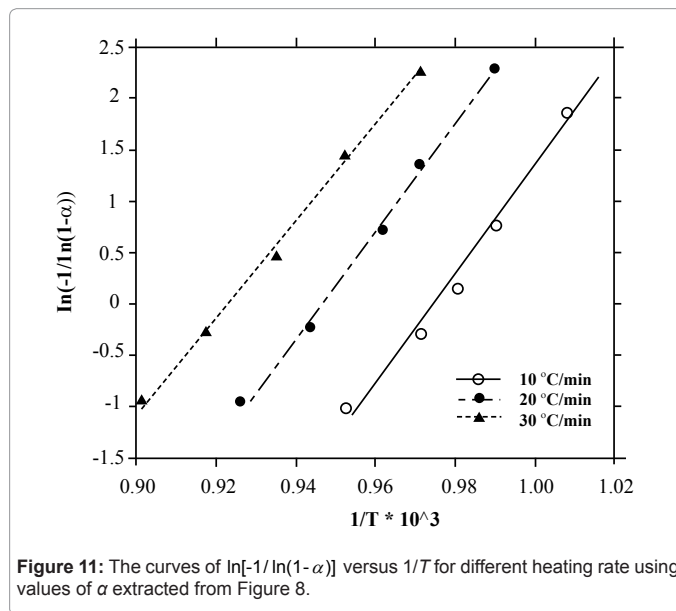


Figure 11: The curves of $\ln[-1 / \ln(1 - \alpha)]$ versus $1/T$ for different heating rate using values of α extracted from Figure 8.

for different heating rates. Then, the Arrhenius parameters at different heating rates are also inserted in table 3 (extracted from figure 11). Therefore, among various gas-solid kinetic models, D2 was identified to be most suitable model for oxidation reaction of aluminum powder particles (through region IV, wherein aluminum is in the form of a melt within the oxide crust) and thus the kinetic triplet was obtained by the method of kinetic analysis. According to table 3, by increasing the heating rate, the activation energy and the pre-exponential factor of the reaction do not change significantly. This means that the reaction

Heating rate (°C/min)	Activation energy (kJ/mol)	A (min ⁻¹)
10	440.3	1.6×10^{23}
20	433.7	0.9×10^{20}
30	430.5	1.6×10^{18}

Table 3: The Arrhenius parameters extracted from Figure 11.

mechanism in a wide range of α values ($0.1 < \alpha < 0.9$), is single-step. Additionally, the obtained average value of the activation energy using this method is in good agreement with values of E , which were determined in studies of Schoenitz et al. [15].

As mentioned in the above paragraphs the identified kinetic model can be justified by the microstructure observations (the experimental study). This fact represents the reliability and accuracy of the method in non-isothermal kinetic analysis.

Based on the results showed above, it is expected that the method can be applicable for both the single-step and multi-step reactions. In other words, application of the method can easily describe the course of multi-step reactions.

Conclusion

The following conclusions can be drawn from this study on the kinetics of the oxidation process of pure aluminum powder particles within the temperature range of 25-1400°C.

The oxidation mechanism

The oxidation of aluminum powders was carried out at different stages. In the initial stage, the rate of oxidation was very negligible. In continuation, the amorphous oxide crust was changed into crystalline phase by increasing the temperature up to the limit of 600°C. Because of the formation of grain boundary in the structure of the crust through crystallization, the oxidation rate is increased. But, by increasing the temperature up to 700°C, the diffusion paths were destroyed by the effect of oxidation process so that the rate of oxidation was abruptly reduced. By increasing the temperature due to expansion of melted aluminum (in 660°C), it created an intense tension on the crust. Within the temperature range of 1000-1150°C, the melt ruptured the crust and permeated outward. The contact of this melt with oxide atmosphere made an intense oxidation. The main stage of the oxidation of aluminum powder particles was oxidized at this stage. In addition, according to the presence of the aluminum remaining in the products, it could be inferred that the complete oxidation process did not take place even up to 1400°C.

The kinetic analysis of oxidation

A new simple method for kinetic analysis of dynamical TG and DTA curves obtained at different heating rates was developed and validated in this study. The method was used to yield the kinetic triplet at any particular value of α . So, based on this method, a kinetic analysis for the main stage of oxidation (within the temperature range of 1000-1150°C) was performed and thus the following kinetic triplet was obtained: $f(\alpha) = -1/\ln(1-\alpha)$, $E \approx 435$ (kJ/mol) and $A \approx 0.9 \times 10^{20}$ (min⁻¹). The kinetic model ($f(\alpha)$; the two-dimensional diffusion controlled model) obtained by the method, displayed a good agreement with the mechanism of the presented in the previous paragraph (the experimental studies). Also, it was found that the gas-solid reaction model was appropriate for the oxidation of aluminum powder.

References

1. Trunov MA, Schoenitz M, Dreizin EL (2005) Ignition of Aluminum Powders Under Different Experimental Conditions. *Propell Explos Pyrot* 30: 36-43.

2. Price EW, Sigman RK (2000) Combustion of aluminized solid propellants. *Solid propellant chemistry, combustion, and motor interior ballistics* (A00-36332 09-28), Reston, VA, American Institute of Aeronautics and Astronautics, Inc. *Progress in Astronautics and Aeronautics* 185: 663-687.
3. Dong H, Zhumei S (1996) Study of the fast reaction characteristics of aluminized PETN explosive powders. *Combust Flame* 105: 428-430.
4. Vahdati Khaki J, Panjepour M, Kashiwaya Y, Ishii K, Sheikhab Bafghi M (2004) *Steel res int* 75.
5. Jeurgens LPH, Sloof WG, Tichelaar FD, Mittemeijer EJ (2000) Thermodynamic stability of amorphous oxide films on metals: Application to aluminum oxide films on aluminum substrates. *Phys Rev B* 62: 4707-4719.
6. Jeurgens LPH, Sloof WG, Tichelaar FD, Mittemeijer EJ (2002) Structure and morphology of aluminium-oxide films formed by thermal oxidation of aluminium. *Thin Solid Films* 418: 89-101.
7. Jeurgens LPH, Sloof WG, Tichelaar FD, Mittemeijer EJ (2002) Composition and chemical state of the ions of aluminium-oxide films formed by thermal oxidation of aluminium. *Surf Sci* 506: 313-332.
8. Jeurgens LPH, Sloof WG, Tichelaar FD, Mittemeijer EJ (2002) Growth kinetics and mechanisms of aluminum-oxide films formed by thermal oxidation of aluminum. *J Appl Phys* 92: 1649-1656.
9. Sanchez-Lopez JC, Gonzalez-Elipe AR, Fernandez A (1998) Passivation of nanocrystalline Al prepared by the gas phase condensation method: An x-ray photoelectron spectroscopy study. *J Mater Res* 13: 703-710.
10. Trunov MA, Schoenitz M, Zhu X, Dreizin EL (2005) Effect of polymorphic phase transformations in Al₂O₃ film on oxidation kinetics of aluminum powders. *Combust Flame* 140: 310-318.
11. Riano OA, Wadsworth J, Sherby OD (2003) Deformation of fine-grained alumina by grain boundary sliding accommodated by slip. *Acta Mater* 51: 3617-3634.
12. Levin I, Brandon D (1998) Metastable Alumina Polymorphs: Crystal Structures and Transition Sequences. *J Am Ceram Soc* 81: 1995-2012.
13. Speyer RF (1993) *Thermal Analysis of Materials*. Marcel Dekker Inc, New York, USA.
14. (2009) *Energetic Materials: Characterization, Modeling and Validation*, 40th International Conference of ICT, June 23-26, Karlsruhe, Federal republic of Germany. Fraunhofer ICT, Germany.
15. Schoenitz M, Patel B, Agboh O, Dreizin EL (2010) Oxidation of aluminum powders at high heating rates. *Thermochim Acta* 507-508: 115-122.
16. Sarangi A, Sarangi B, Ray HS, Misra S (1991) Derivative Differential Thermal Analysis (DDTA): In Kinetic Studies of Aluminothermic Reduction. *J Therm Anal* 36: 513-527.
17. Haines PJ (2002) *Principles of thermal analysis and calorimetry*. Royal society of chemistry Cambridge, UK.
18. Brown ME, Maciejewski M, Vyazovkin S, Nomen R, Sempere J, et al. (2000) Computational aspects of kinetic analysis : Part A: The ICTAC kinetics project-data, methods and results. *Thermochim Acta* 335: 125-143.
19. Maciejewski M (2000) Computational aspects of kinetic analysis. Part B: The ICTAC Kinetics Project - the decomposition kinetics of calcium carbonate revisited, or some tips on survival in the kinetic minefield. *Thermochim Acta* 355: 145-154.
20. Vyazovkin S (2000) Computational aspects of kinetic analysis PartC: The ICTAC Kinetics Project—the light at the end of the tunnel? *Thermochim Acta* 355: 155-163.
21. Burnham AK (2000) Computational aspects of kinetic analysis.: Part D: The ICTAC kinetics project-multi-thermal-history model-fitting methods and their relation to isoconversional methods. *Thermochim Acta* 355: 165-170.
22. Roduit B (2000) Computational aspects of kinetic analysis.: Part E: The ICTAC Kinetics Project-numerical techniques and kinetics of solid state processes. *Thermochim Acta* 355: 171-180.
23. Sewry JD, Brown ME (2002) "Model free" kinetic analysis? *Thermochim Acta* 390: 217-225.
24. Maleki A, Panjepour M, Niroumand N, Meratian M (2010) Mechanism of zinc oxide-aluminium aluminothermic reaction. *J Mater Sci* 45: 5574-5580.